Earth Systems and Environment (2019) 3:139–152
https://doi.org/10.1007/s41748-018-0079-1

ORIGINAL ARTICLE

Dust Detection and Aerosol Properties Over Arabian Sea Using MODIS Data

Jyotsna Singh[1,2] · Yoo-Jeong Noh[3] · Shefali Agrawal[1] · Bhishma Tyagi[4]

Received: 2 May 2018 / Accepted: 8 November 2018 / Published online: 17 November 2018

Abstract
The present study deals with the use of Moderate Resolution Imaging Spectroradiometer (MODIS) thermal infrared bands in the dust detection. Eight dust storm cases over the Arabian Sea have been selected (four TERRA and four AQUA) during the year 2002–2008. The brightness temperature (BT) difference method has been applied on MODIS thermal bands 29 (8 µm), 31 (11 µm) and 32 (12 µm) to detect dust storms over the Arabian Sea. The performance assessment of BT differences (BT_{29}–BT_{31} and BT_{31}–BT_{32}) has shown that BT_{31}–BT_{32} has performed better to BT_{29}–BT_{31}. We suggest that BT_{31}–BT_{32} is an effective combination of MODIS bands for dust detection over oceans and sea. The maximum (Dmax) and minimum dust (Dmin) intensity locations have also been identified in all the eight dust storm cases. The aerosol properties (aerosol optical thickness, τ; asymmetry factor g and Angstrom exponent α) over Dmax and Dmin have been studied using MODIS Level 2 data. In AQUA dust storms cases τ values (Dmax) were higher than TERRA dust cases, whereas g values were nearly same. The α was always positive in case of TERRA dust cases; however in AQUA negative α was also reported. Afternoon dust storms are more intense compared to forenoon dust storms and dust particles are also coarser.

Keywords Dust detection · BT difference · Dust aerosol properties · MODIS · Arabian Sea

1 Introduction

The World Meteorological Organization has classified dust into four categories based on the visibility: dust in suspension, blowing dust, dust storm and severe dust storm (Shao 2008). The wind speed varies from light to very strong, whereas the visibility reduces from dust in suspension to severe dust storms. Dust storms mainly originate in arid and semiarid areas. In a dry climate, low soil moisture makes the soil more susceptible to erosion and soil gets easily eroded by wind or flood. Usually, the bigger particle travels a less distance and falls near the source, but smaller particles are carried at a longer distance (thousands of kilometers). Sometimes even larger particle also travels a large distance because of the high wind speed (Betzer et al. 1988). More events of droughts and escalated rate of desertification are responsible for more dust storms (Taghavia and Mohammadi 2008). Dust particle concentration in the atmosphere increases during dust storms, which affect our daily life, aviation and surface transport. It alters the air quality, and it is also a health hazard (Reed and Nugent 2018; Kaiser 2005; Chen et al. 2004). Dust storms also influence the weather and climate on local, regional and global scales (Al-Maamary et al. 2017; Shi and Zhao 2003). The dust aerosols affect the radiative balance of the Earth as it absorbs as well as reflect the incoming solar radiation (Butt et al. 2017; Stocker et al. 2013).

There are different methods of dust storm monitoring—field observations (Christopher and Jones 2010; Kurosaki et al. 2011), lagrangian model-based trajectories and dispersion studies (Lee et al. 2010), and the satellite data analysis (Zhang et al. 2006; Norton et al. 1980). Dust storms in south-west Asia have been observed by (Middleton 1986) using ground station observations. Over land, aerosol

✉ Jyotsna Singh
jsinghenv@gmail.com

[1] Indian Institute of Remote Sensing, Indian Space Research Organisation, Department of Space, Government of India, Dehradun, India

[2] Present Address: Shanti Raj Bhawan, Paramhans Nagar, Kandwa, Varanasi 221106, India

[3] Cooperative Institute for Research in the Atmosphere, Colorado State University, Fort Collins, CO 80523, USA

[4] Department of Earth and Atmospheric Sciences, National Institute of Technology Rourkela, Rourkela 769008, India

observations are present (Sateesh et al. 2018; Kiran et al. 2018); however, over ocean and sea, it is difficult to set up the dust aerosol observational network. Many scientific studies over these areas were done using cruises (Moorthy et al. 2005; Babu et al. 2004). These cruise experiments are expensive, suitable for short-term observation and hence cannot be performed at regular intervals. This has limited the aerosol information over sea and ocean. The variability in dust frequency and intensity can also be understood by dust emission and transport modelling. In 1999, U.S. Navy has developed Navy Aerosol Analysis and Prediction System (NAAPS)—a first operational dust forecast model (Lee et al. 2017). Later on, operational dust storm forecast model has also been developed by different Meteorological organizations across the world like UK Met Office (for south Asia since April 2008 and globally since 2011) (http://forecast.uoa.gr/Dust-wshop-pdf/Brooks.pdf) and Barcelona Dust Forecast Center for Northern Africa, Middle East and Europe (https://dust.aemet.es/about-us/report-2015). These operational dust storm forecast models are breakthrough towards the dust forecasting. However, forecast evaluation results indicated that there is a need to improve them further [https://dust.aemet.es/forecast-evaluation (2017)].

The third approach to study dust storm is the use of satellite images. For studying the lifecycle and properties of dust storms events, remote sensing is better than ground observation because of its global coverage (Xie et al. 2017). Satellite data cover a broad geographical area (Singh 2016) and can be integrated with model simulations to improve the capabilities of model forecasting (Yu and Yang 2016). Many satellite images such as NOAA-Advanced High-Resolution Radiometer (AVHRR) (Janugani et al. 2009; Zhu et al. 2007), METEOSAT data (Legrand et al. 2001) and Landsat Thematic Mapper (TM)/Enhanced Thematic Mapper (ETM) (Wang et al. 2013) were used for studying dust storms. Total Ozone Mapping Spectrometer (TOMS) has been used to detect major dust source regions on a global scale (Washington et al. 2003). Several techniques, such as the optical (Norton et al. 1980) and thermal infrared (TIR) (Ackerman 1989) spilt window technique, have been used by scientists since 1970s to study dust storms. Among these two, TIR has shown better results over surfaces with high albedo and night times in dust storm detection. The TIR channels also work well for dust detection over land and ocean. The amount of energy emitted by surface features is easy to detect in TIR range irrespective of the time of the day. One thermal channel (11 μm) of Nimbus has been used by (Shenk and Curran 1974) for the dust detection. This one channel method misinterpreted clouds as dust as brightness temperature (BT) changes are affected by surface emissivity. In the past, Moderate Resolution Imaging Spectroradiometer (MODIS) (high spectral and temporal resolution) has been widely used to detect dust storm over the globe using thermal channels (Jafari and Malekian 2015; Karimi et al. 2012; Zhang et al. 2008). Dust indices like BT difference and normalized difference dust index (NDDI) using MODIS channels have been used to detect dust storms (Zhang et al. 2008). BT difference is more reliable for dust source detection (in several situations such as multi-plume and multi mineralogical conditions) than NDDI and optical-based algorithms (Yue et al. 2017). The dust could be easily detected using BT difference technique compared to the visible scene (Baddock et al. 2009). The use of two MODIS thermal channels (11–12 μm) instead of one thermal band showed higher accuracy (Li and Song 2009). It has been observed that BT difference of 11–12 μm was always negative for dust while 8.5–11 μm ranged from positive to negative based on dust concentration (Zhang et al. 2006).

To understand the variation of aerosols over any region, detailed knowledge of aerosols physical and optical properties is required. This information is sparse over oceans and sea. Therefore, over these areas, satellite remote sensing techniques can be used to detect dust storms and study aerosol properties. Stratospheric volcanic aerosols detection over oceans using three thermal channels (8 μm, 11 μm and 12 μm) have proposed that the uniform surface of Ocean has an advantage over land to aerosols detection as the spectral variation of surface emissivity complicates the aerosol detection over land (Ackerman 1997).

The continental area around the Arabian Sea (the alluvial plains of southern Iraq and Kuwait, the southern Arabian Peninsula (Oman, Yemen, Rub-Al-Khali), the Somali Coast, India, Pakistan, and Iran) is the principal sources for the production of dust (Middleton 1986; Pease et al. 1998). The massive dust production over these regions makes these continental areas and the Arabian Sea as a high dust load area (Kolla and Biscaye 1977; Sirocko 1991). The higher dust aerosols over Arabian Sea impact Indian summer monsoon (Solmon et al. 2015). Over the Arabian Sea, these dust aerosols are also the primary source of sediments. It has been suggested that mineral dust supplies nutrients to the ocean and influences the primary productivity of ocean (Betzer et al. 1988; Coale et al. 1996; Martin et al. 1994).

The goal of the present paper is to study the use of satellite data in the dust storm detection over the Arabian Sea, which has been fulfilled by the following objectives: (1) To detect the dust spatially and study aerosol properties of the dust storms over the Arabian Sea using MODIS data and (2) To identify the maximum (Dmax) and minimum (Dmin) dust aerosol locations from the spatially detected dust storms. The aerosol properties of these regions were also studied.

2 Study Region and Datasets

2.1 Location and Climatic Details of the Study Area

In the present study, the Arabian Sea area near the North Western part of India has been selected for detecting the dust storms (Fig. 1).

The winds over Arabian Sea show reversal of wind direction and speed that causes a drastic change in rainfall intensity. These changes in weather phenomena affect the Indian monsoon and its climate (Krishnamurthy and Kinter 2003). The densely populated India also serves as the source of anthropogenic pollutants and affects the meteorology of Arabian Sea. Therefore, it is worthy to study dust storm over this area. There are two distinct seasons over the Arabian Sea, winter monsoon season (WMS) and summer monsoon season (SMS) (Satheesh et al. 2006). The variation of meteorological parameters in these two seasons is given in Table 1. The WMS prevails from November to March and SMS from April to September. The average wind speed is less than 5 m/s and it blows predominantly from North/North-easterly in WMS whereas in SMS South-westerly wind blow at higher wind speed

Fig. 1 Google Earth image of Arabian Sea and surrounding continental areas' contributors of dust over the Arabian Sea (Pease et al. 1998) http://www.earth.google.com; imagery date December 14, 2015

Table 1 Variation of meteorological parameters in two seasons over the Arabian Sea (Satheesh et al. 2006)

S. no		Winter monsoon season (WMS)	Summer monsoon season (SMS)
1	Month	November–March	April to September
2	Wind direction	North/North-easterly	South-westerly/Westerly
3	Wind speed	< 5 m/s	10–15 m/s
4	Advection	Indian landmass	Ocean and western landmass
5	Cloud condition	Nearly clear	Cloudy
6.	Rainfall	Low	High

(10–15 m/s). In WMS, advection from the Indian landmass is important and in SMS, advection from the ocean and western landmass plays an important role. The cloud remains nearly clear in WMS that leads to low rainfall, but in SMS cloudy situation exists that causes the heavy rainfall which also covers the Indian subcontinent. The present work focuses only on the dust storm cases during WMS over the Arabian Sea, as in this season sky remains nearly clear of clouds and residence time of pollutants in the atmosphere increases, hence providing good conditions for studying dust aerosols (Satheesh et al. 2006).

Table 3 Details of selected dust storm cases over the Arabian Sea

S. no	Satellite	Date	Julian Day	Time
1.	TERRA	25 Jan 2002	25	06:15
2.	TERRA	14 Dec 2003	348	06:15
3.	TERRA	10 Feb 2007	41	06:00
4.	TERRA	02 Feb 2008	33	06:20
5.	AQUA	03 Feb 2003	34	08:40
6.	AQUA	14 Dec 2003	348	09:20
7.	AQUA	09 Feb 2004	40	09:10
8.	AQUA	13 Nov 2008	318	09:00

2.2 Datasets

The MODIS data have been used to detect the dust storm in the present study. The MODIS sensor is carried on both the satellites (TERRA and AQUA). It is launched by NASA in 1999 (TERRA) and 2002 (AQUA). The details of remote sensing data used in the present study are given in Table 2. The MODIS captures data in 36 spectral bands "(0.4–14.4 μm)". The spatial resolutions of MODIS are "250 m, 500 m and 1 km". Out of 36 spectral bands, 11 bands are in the visible range, 9 in the near-infrared (NIR), 6 in the TIR, 4 in the shortwave infrared (SWIR), and 6 in the long wave infrared range (LWIR).

The daily MODIS Level 1B (MOD021KM-Level 1B Calibrated Radiances-1 km (TERRA) and MYD021KM—Level 1B Calibrated Radiances-1 km (AQUA) and Level 2 data [MOD04_L2-Level 2 Aerosol (TERRA) and MYD04_L2-Level 2 Aerosol (AQUA)] have been downloaded from the site LAADS website (https://ladsweb.modaps.eosdis.nasa.gov). Level 2 MODIS data used in the present study are Aerosol Optical Thickness (AOT) (τ) at 550 nm, asymmetric factor (g) at 550 nm and 550–865 μ based Angstrom exponent (α). The details of different dust cases are given in Table 3. As per the τ availability, total eight dust storm cases (four TERRA and four AQUA) for WMS have been selected.

3 Methodology

3.1 Processing of MODIS Data

The MODIS Level 1B product is available for any part of the world since 2000. However, to use these data in the further analysis, it is necessary to convert these data into radiance, surface reflectance or BT. The Level 1B data are converted into the BT (degrees Kelvin) using MODIS Conversion Tool Kit (MCTK) (https://github.com/dawhite/MCTK). MODIS Level 2 data (τ, g, α) were also projected using MCTK. This method of processing of MODIS data (Level 1 and Level 2) is used in many previous studies (Duan et al. 2017; Karimi et al. 2016; Munir et al. 2015).

3.2 Dust Detection Methodology

The methodology for detecting dust and analysis has been shown in Fig. 2. In the present work, the combination of 8–11 μm and 11–12 μm has been tried to detect the dust over the ocean. The performance of both the combination has been tested by scatter plots and histograms (explained in Sect. 4.1). In MODIS data, 8 μm, 11 μm and 12 μm correspond to the band number 29, 31 and 32, respectively. Hereafter, BT difference of 8–11 μm and 11–12 μm is represented as BT_{29}–BT_{31} and BT_{31}–BT_{32}, respectively.

Table 2 Characteristics of Moderate Resolution Imaging Spectroradiometer (MODIS) data used in the present study

S. no	Data type	Satellites	Spatial Resolution at Nadir	Data archive	Overpass time
Level 1					
1	MOD02	TERRA	1 km "(TIR + all bands)"	1999-date	10:30 AM
2	MYD02	AQUA	1 km "(TIR + all bands)"	2002-date	13:30 PM
Level 2					
3	MOD04	TERRA	10 km	1999-date	10:30 AM
4	MYD04	AQUA	10 km	2002-date	13:30 PM

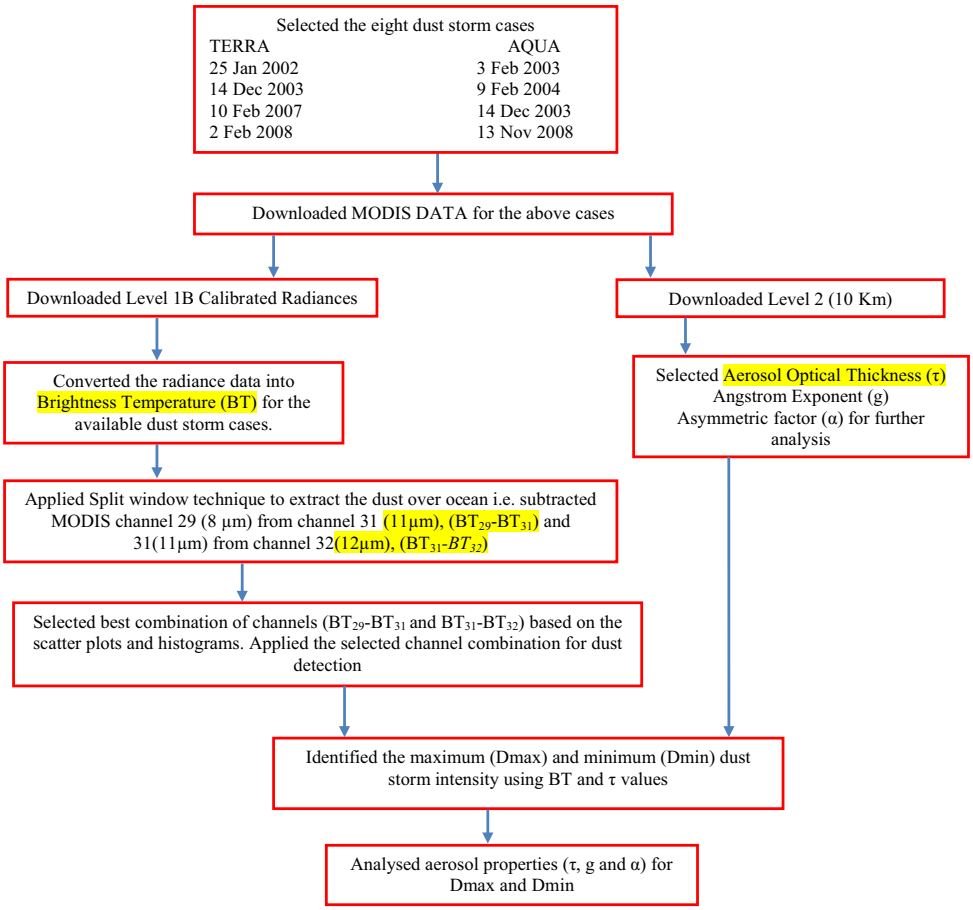

Fig. 2 Methodology used in the present work

4 Results and Discussion

4.1 Performance of BT Difference (BT_{29}–BT_{31} and BT_{31}–BT_{32}) for the Detection of Dust

In the present work, BT difference of BT_{29}–BT_{31} and BT_{31}–BT_{32} has been tested for the suitability of the proper combination of the channel for the detection of dust. In Fig. 3, scatter plots of BT_{29}–BT_{31} and BT_{31}–BT_{32} are shown for the dusty and clear condition for one TERRA (25 Jan 2002) and one AQUA (3 Feb 2003) dust cases.

The dust and clear regions used for plotting scatter plots and histograms are shown in Fig. 4e for TERRA and Fig. 5e for AQUA. The points of dust and clear are shown in red and black color, respectively. The BT_{29}–BT_{31} and BT_{31}–BT_{32} ranged between −1.6 and −2.3 and −0.3 to 0.2 in case of dust and −2.4 to −3.2 and 0.3–0.7 for clear, respectively (Fig. 3a, c). Here, one point is interesting to note that in BT_{29}–BT_{31} both dust (−1.6 to −2.3) and clear (−2.4 to −3.2) pixels have the values in the negative range (Fig. 3a) and but in BT_{31}–BT_{32} clear pixels have shown the positive values (0.3–0.7) (Fig. 3c); sometimes these values were even more than 1 (Fig. 3g). The dust pixels have values always less than 1 (Fig. 3c, g) and in case of thick dust, values are in the higher negative range (BT_{31}–BT_{32}). The negative value in BT_{31}–BT_{32} for dust has been reported in many studies (Vincent 2018; Yue et al. 2017). In case of BT_{29}–BT_{31}, the dust and clear points are more scattered, and the distance between the clear and dust clusters is less (Fig. 3a). However, BT_{31}–BT_{32} channel difference was less scattered and the distance between the clear and dust clusters is more (Fig. 3c). This fact is more pronounced in Fig. 3e where in case of BT_{29}–BT_{31} the clear and dust points have been overlapped and made it very difficult to detect dust from the imagery. However, in case of BT_{31}–BT_{32}, the clear and dust clusters are largely separated from each other (Fig. 3g).

The scatter plot results have been supported by the histogram of BT difference of the dusty area where the two modes of histogram have been observed in case of BT_{29}–BT_{31} (Fig. 3b, f) and unimodal distribution in case of BT_{31}–BT_{32} (Fig. 3d, h). The bimodal distribution shows that the samples are collected from the two different populations and the higher peak show the population of dust clusters and lower peak shows the mixed population. However, in case of BT_{31}–BT_{32}, only one peak has been observed that shows the presence of one population (i.e. dust) (Fig. 3d, h). Based on these results, it can be suggested that BT_{31}–BT_{32}

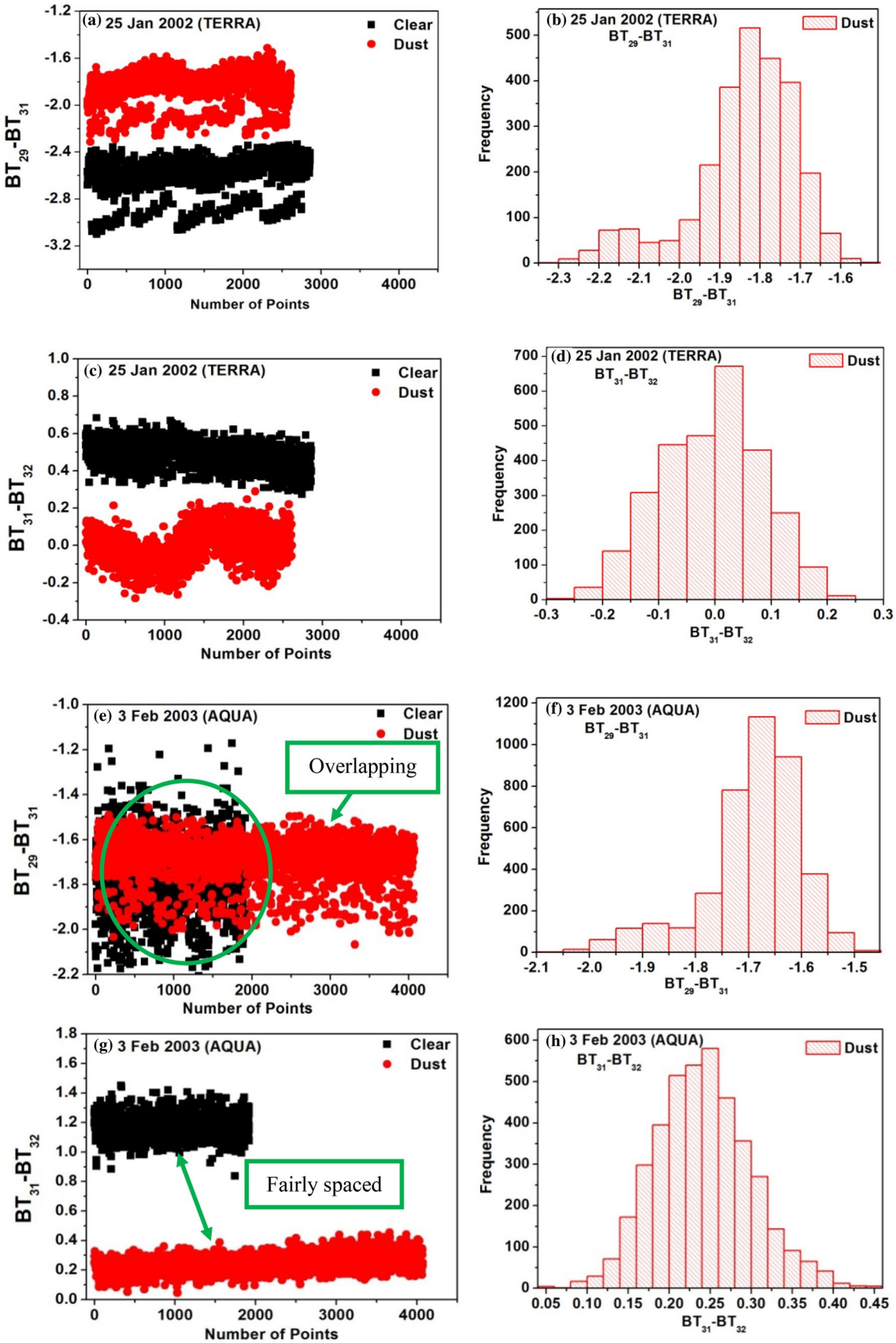
(a) 25 Jan 2002 (TERRA)
Clear
Dust
BT29-BT31
Number of Points
(b) 25 Jan 2002 (TERRA)
BT29-BT31
Dust
Frequency
BT29-BT31
(c) 25 Jan 2002 (TERRA)
Clear
Dust
BT31-BT32
Number of Points
(d) 25 Jan 2002 (TERRA)
BT31-BT32
Dust
Frequency
BT31-BT32
(e) 3 Feb 2003 (AQUA)
Clear
Dust
Overlapping
BT29-BT31
Number of Points
(f) 3 Feb 2003 (AQUA)
BT29-BT31
Dust
Frequency
BT29-BT31
(g) 3 Feb 2003 (AQUA)
Clear
Dust
Fairly spaced
BT31-BT32
Number of Points
(h) 3 Feb 2003 (AQUA)
BT31-BT32
Dust
Frequency
BT31-BT32

◂**Fig. 3** Scatter plots (**a**, **c**, **e** and **g**) and Histograms (**b**, **d**, **f** and **h**) of Brightness Temperature (BT) difference between BT_{29}–BT_{31} and BT_{31}–BT_{32} for 25 Jan 2002 (TERRA) and 3 Feb 2003 (AQUA)

has performed better to BT_{29}–BT_{31} for the dust extraction from MODIS (TERRA and AQUA) images. The BT_{31}–BT_{32} have more potential to separate thick dust from the cloud and other atmospheric particles. The more negative value in BT difference image indicates thick dust (more τ values) and vice versa. The present result of dust extraction is coherent with the study conducted by (Ackerman 1997).

We have used BT_{31}–BT_{32} for the dust detection for dust storm cases. Along with BT difference MODIS Level 2, τ values have also been used to analyse the area of a dust storm in BT difference image by BT_{31}–BT_{32}. In Fig. 4, the true colour, BT_{31}–BT_{32} and τ values have shown for the better understanding of spatially dust detected area. The region in red and purple indicates the higher and lower values of τ, respectively. In all the dust storm cases, MODIS τ and BT_{31}–BT_{32} have shown good coherence. The area shown in black represents the missing data. Sometimes due to some error in the satellite, the data are not recorded that cause the loss of information. Over Arabian Sea, a dust storm is a common phenomenon, and it is detected spatially very well by BT_{31}–BT_{32} difference method in both TERRA (Fig. 4) and AQUA (Fig. 5) dust storm images.

4.2 Dust Aerosols Properties in Selected Dust Storm Cases

4.2.1 Variation in τ

The variation of τ has been shown in (Fig. 6a, b) for dust storm cases captured by MODIS TERRA and AQUA, respectively. In case of TERRA, τ values were less for the dust storm event occurred on 25 Jan 2002 ($\tau < 1.3$) and 10 Feb 2008 ($\tau < 1.5$) compared to dust storm events 14 Dec 2003 where sometimes $\tau > 2.8$ and 2 Feb 2008 ($\tau > 2.4$) (Fig. 6a). Over the Arabian Sea, many intense dust storm occurs resulting in high τ. In AQUA, the least τ values were recorded for 3 Feb 2003 ($\tau < 0.87$) and in all the other dust cases τ values crossed 2.4. The local time of AQUA overpass is around 13:30 PM. In the afternoon intense dust storm activities take place which increase the number of dust aerosols in the atmosphere and, hence, τ values are higher in AQUA (Fig. 6b) compared to TERRA (Fig. 6a).

4.2.2 Variation in α

The α provides the information of particle size. The smaller values of α indicate the larger particle size and vice versa (Levy et al. 2009). In the present study, the majority of α values were less than 0.5. In case of TERRA, only a few values of dust storm cases: 25 Jan 2002 and 10 Feb 2007 have crossed 0.6 (Fig. 6c). However, in case of AQUA dust storm, almost all α values were less than 0.6 (Fig. 6d). At this point, it is worth to be noted that size of the dust aerosols originated in the afternoon dust storms were slightly larger compared to the morning time. It might be due to the intense heat that decreases the moisture level in the soil. The loosely bounded large soil particles are also easily lifted into the atmosphere by the strong wind.

4.2.3 Variation in g

The g gives us the idea of the scattering direction, i.e. either forward or backwards in the light striking the aerosol particles. As per the literature, $g > 0$ indicates light scattering in the forward direction (Levy et al. 2009) and 'g' values approaching +1 shows the presence of larger dust particles (Mie particle). In case of $g = -1$, then its scattering direction is backward. In the present work for the dust storm cases captured by TERRA, g varied in between 0.66 and 0.78 (Fig. 6e), and for AQUA it varied between 0.64 and 0.79 (Fig. 6f).

For TERRA images, the highest 'g' value was reported for dust storm case, 2 Feb 2002 ($g = 0.78$) and for AQUA images g was highest for dust case 13 Nov 2008. Here, for both AQUA and TERRA dust cases 'g' value has been found to be positive and, in some cases, it was even more than 0.7, the dust aerosols in these dust storm cases are Mie particles.

4.3 Aerosol Properties in Maximum and Minimum Dust Storm Locations

After successful detection of the dust storm over the Arabian Sea for the eight dust storm cases, Dmin and Dmax dust locations have been identified using BT_{31}–BT_{32} and τ values in the dust storm cases (Fig. 7).

Dust aerosols properties (τ, g and α) have been studied for Dmax and Dmin dust aerosol locations. The τ value in Dmax was maximum for AQUA dust cases, 13 Nov 2008 ($\tau = 3.286$) and minimum for 3 Feb 2003 ($\tau = 0.865$) (Table 4). The g value was also high in the case of 13 Nov 2008 ($g = 0.781$). The dust aerosol properties of a dust storm (Dmax) occurred on 13 Nov 2008 indicate that these dust particles favor the forward scattering and their size was also large ($\alpha = -0.19$) (Table 4). The negative value of α indicates the presence of coarse particles (Kaskaoutis et al. 2009). Likewise, the aerosol properties of dust aerosol in different dust events have been given in Table 4. The intensity of the dust storm occurred on 13 Nov 2008 (AQUA) has been well recorded in BT_{31}–BT_{32} images (Fig. 5).

In the present work, α for most of the dust has ranged below or equal to 0.64 except 14 Dec 2003 (0.765). It has been reported that α ranges from 1.2 for the area near

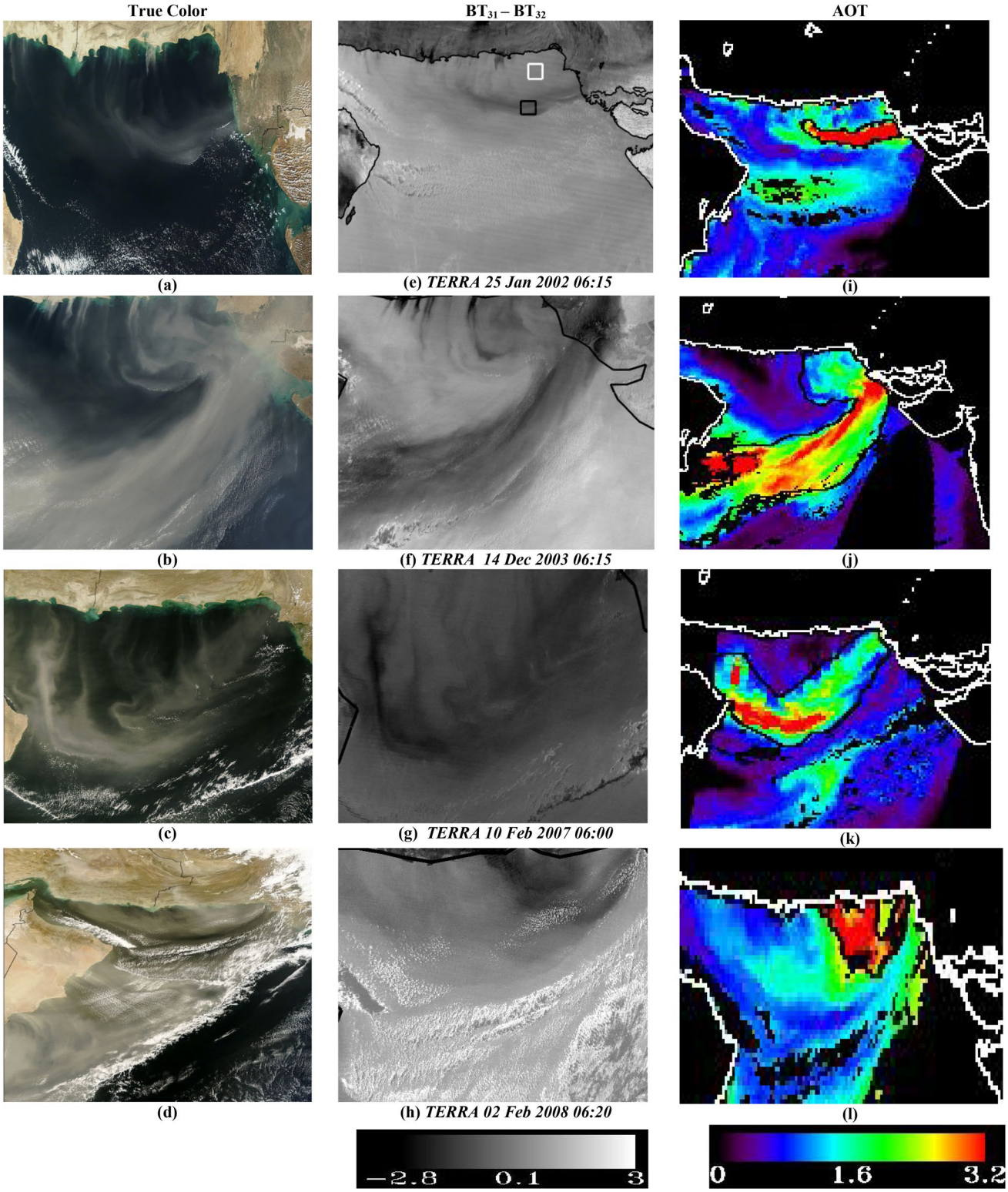

Fig. 4 The true color (**a**–**d**), Brightness Temperature (BT) difference (BT_{31}–BT_{32}) (**e**–**h**) and Aerosol Optical Thickness (AOT) (τ) (**i**–**l**) values in different dust storm cases captured by TERRA. Date and time of dust cases are written in Italics in centre. Black and white boxes represent dust and clear area, respectively, for dust case TERRA 25 Jan 2002 used for scatter plot and histogram. In τ images, dust storm area used for aerosol properties analysis is marked with a black polygon

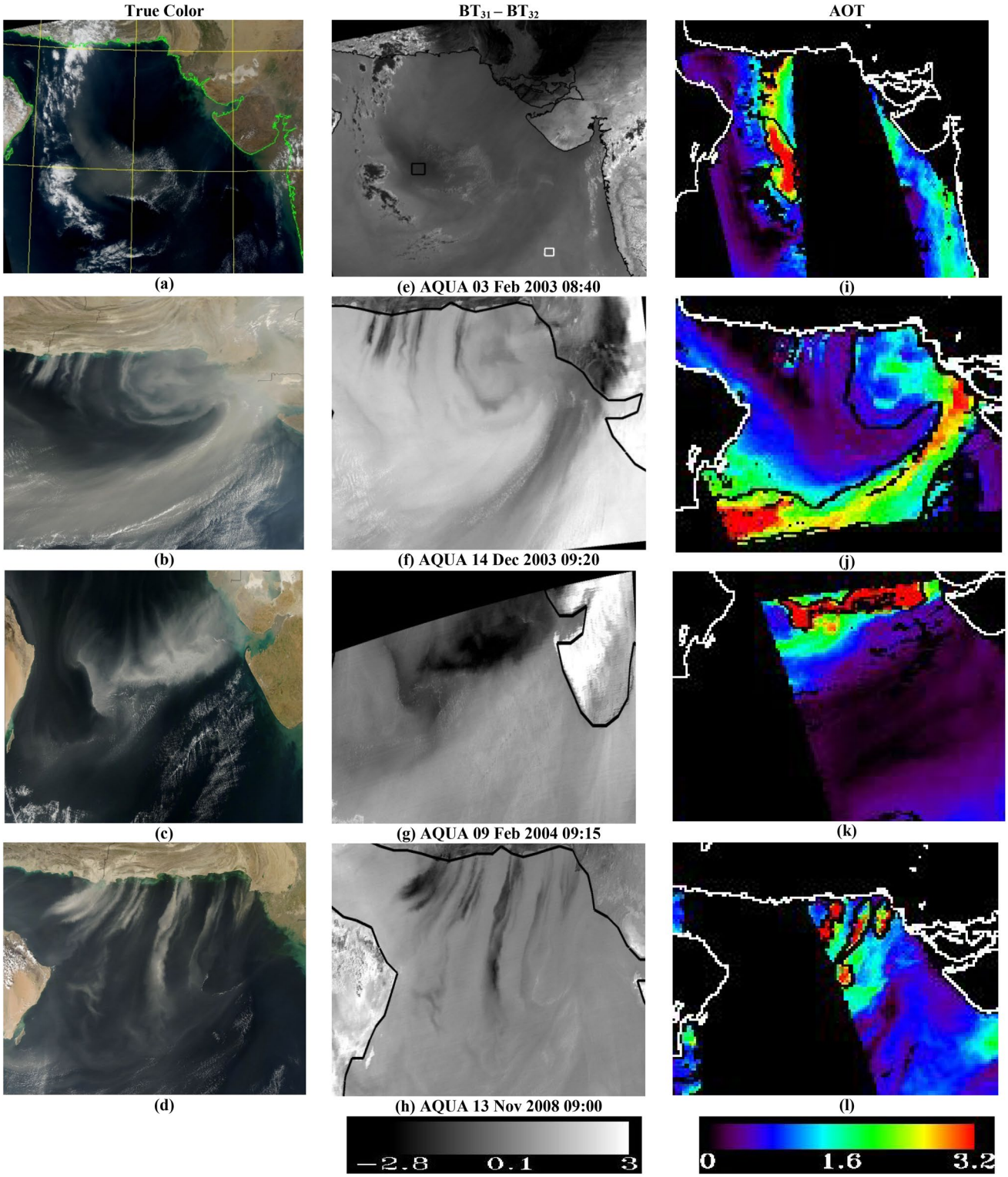

Fig. 5 The true color (**a**–**d**), brightness temperature (BT) difference (BT_{31}–BT_{32}) (**e**–**h**) and Aerosol Optical Thickness (AOT) (**i**–**l**) values in different dust storm cases captured by AQUA. Date and time of dust cases are written in italics in centre. Black and white boxes represent dust and clear area, respectively, for dust case AQUA 3 Feb 2003 used for scatter plot and histogram. In τ images, dust storm area used for aerosol properties analysis is marked with a black polygon

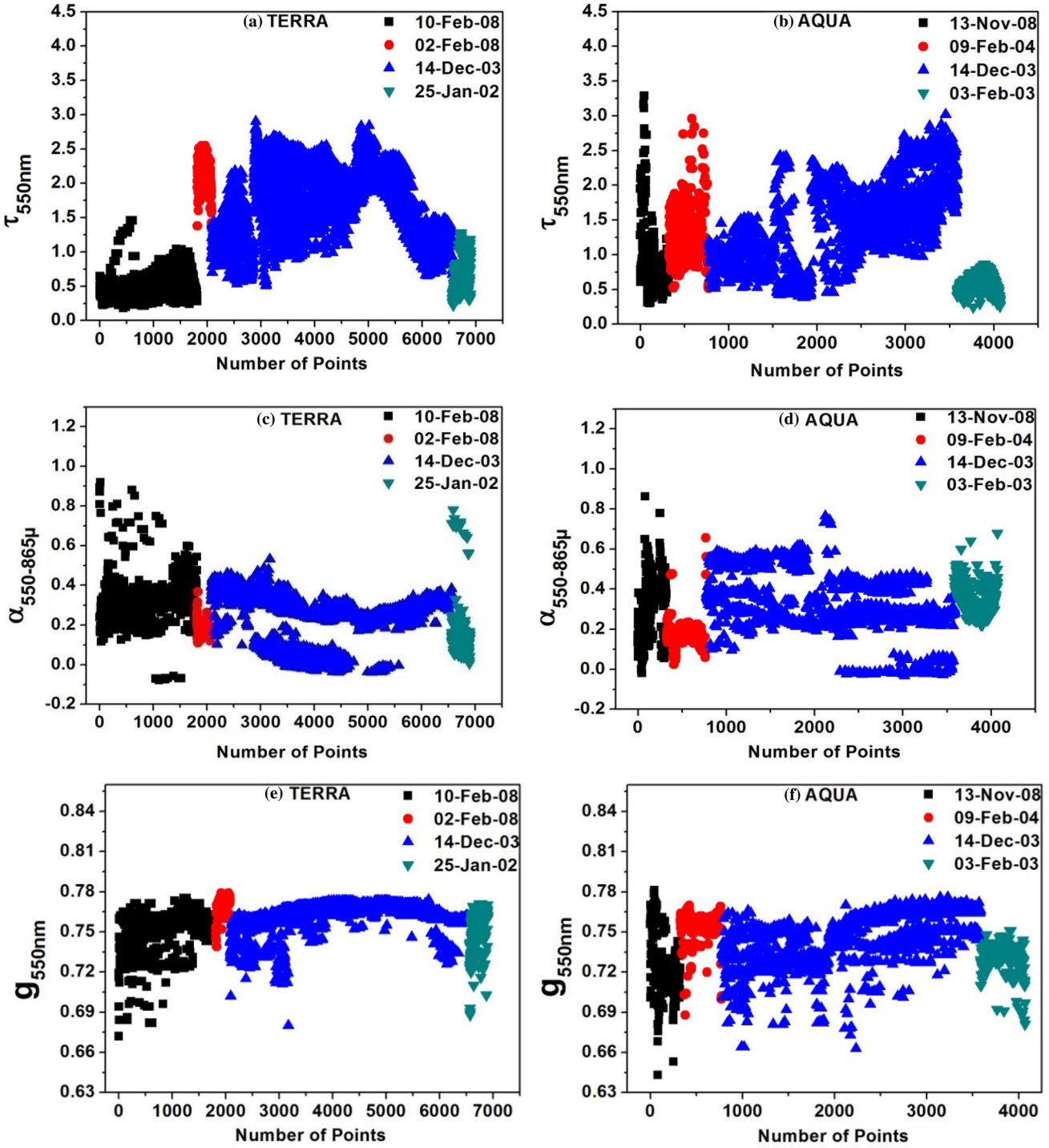

Fig. 6 Variation in aerosol optical thickness at 550 nm (τ), Angstrom exponent 550–865μ (α) and asymmetric factor at 550 nm (g) in TERRA and AQUA dust storm cases

coastal region and 0.6 in remote oceanic regions (Satheesh and Moorthy 1998). The results of α are in agreement with the α values reported by them. The range of g has been reported 0.7 (Dmin) and 0.78 (Dmax) in the selected dust cases. The g value for the maritime dust aerosol has been reported by Chou et al. (2002) in the range of 0.78–0.79. The g value for dust aerosol in the present study has been found to be in the similar range in case of Dmax.

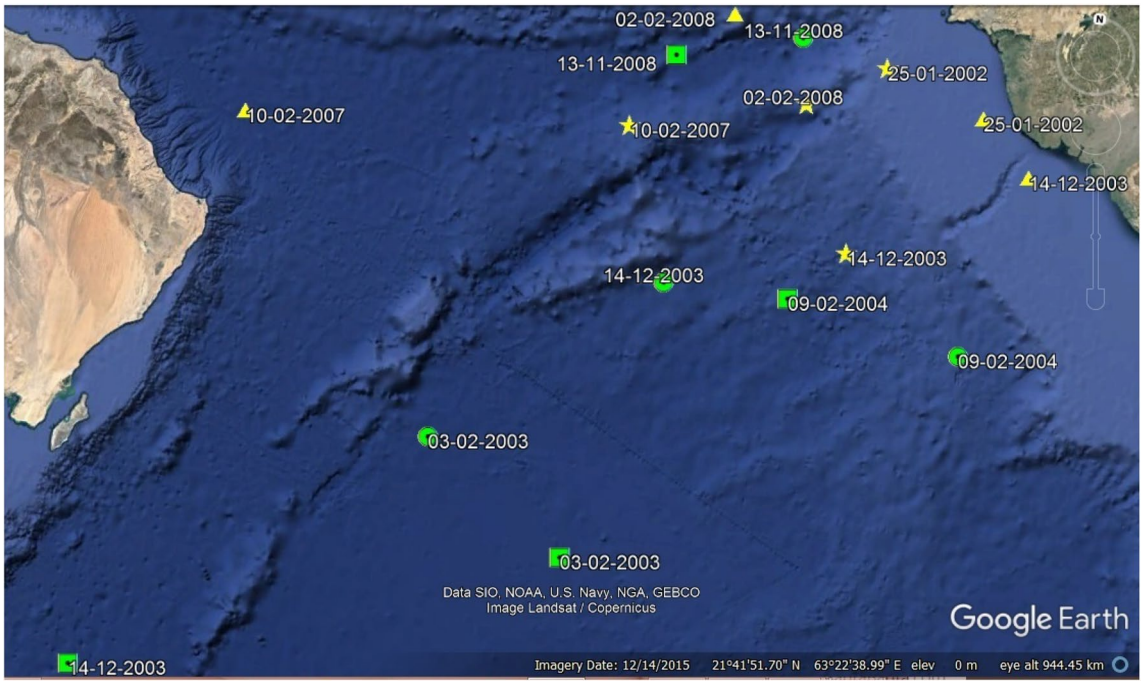

Fig. 7 TERRA and AQUA maximum (Dmax) and minimum (Dmin) dust storm locations with dates http://www.earth.google.com; imagery date December 14, 2015 [*Symbols triangle, star, black dot square and black dot circle represent TERRA maximum, TERRA minimum, AQUA maximum and AQUA minimum locations, respectively (*Source* Google earth image)]

Table 4 Aerosol properties of maximum (Dmax) and minimum (Dmin) dust intensity

S. no	Dust cases	Latitude	Longitude	AOT (τ)	Asymmetry factor (g)	Angstrom exponent (α)
1.	*25-Jan-02*					
	Dmin	24.35	66.10	0.221	0.726	0.123
	Dmax	23.99	67.07	1.276	0.745	0.238
2.	*14-Dec-03*					
	Dmin	22.70	65.854	0.506	0.731	0.333
	Dmax	23.51	67.553	2.9	0.764	0.104
3.	*10-Feb-07*					
	Dmin	23.61	63.70	0.179	0.753	0.598
	Dmax	23.35	60.35	1.456	0.771	0.176
4.	*02-Feb-08*					
	Dmin	23.96	65.35	1.37	0.76	0.194
	Dmax	24.68	64.59	2.546	0.771	0.142
5.	*03-Feb-03*					
	Dmin	20.74	62.16	0.244	0.692	0.639
	Dmax	19.83	63.491	0.865	0.738	0.247
6.	*14-Dec-03*					
	Dmin	22.29	64.17	0.383	0.727	0.227
	Dmax	18.31	59.04	3.016	0.767	0.066
7.	*09-Feb-04*					
	Dmin	21.90	67.26	0.516	0.702	0.561
	Dmax	22.26	65.34	2.957	0.761	0.232
8.	*13-Nov-08*					
	Dmin	24.54	65.26	0.302	0.713	0.613
	Dmax	24.27	64.07	3.286	0.781	−0.019

5 Conclusions

A total of eight dust storm cases (four TERRA and four AQUA) have been selected for the study of dust storms. The dust detection analysis has been performed using BT difference technique. The BT imageries were obtained from the MODIS TIR bands 8 μm (Band number 29), 11 μm (Band number 31) and 12 μm (Band number 32). The two-channel BT difference dust detection methods involve the combination of mainly three BT bands (BT_{29}–BT_{31} and BT_{31}–BT_{32}). The values were always negative (degree Kelvin) for clear as well as dust-laden atmosphere in the scatter plot of BT_{29}–BT_{31}. However, in case of BT_{31}–BT_{32}, clear pixels have always shown the positive value of clear sky and thick dust have always shown negative values. Histogram of dust points was bimodal in case of BT_{29}–BT_{31} and unimodal in case of BT_{31}–BT_{32}. The MODIS Level 2 data have been used to study the aerosol properties like τ, α and g. Generally, in the afternoon dust cases (AQUA), τ values were higher compared to forenoon dust storm cases (TERRA). The g values were nearly similar for TERRA and AQUA images ($g > 0.6$). The positive value of g indicates the forward scattering of light by the aerosol particles. The value of α was less than 0.4 for most of the TERRA dust cases; only a few have crossed 0.6 marks. However, in AQUA almost all the dust cases have α below 0.6. Based on the analysis, the findings can be summarized as:

- BT_{31}–BT_{32} performed well compared to BT_{29}–BT_{31} in the spatial detection of the dust storm events over the Arabian Sea.
- MODIS Level 1 data have a good spatial and temporal coverage of the dust storm in both forenoon (TERRA) and afternoon (AQUA). The TIR MODIS Level 1 data can be used efficiently in studies related to a dust storm.
- The aerosol properties extracted from MODIS Level 2 aerosol data have good coherence with the aerosol observational data collected by different groups of a researcher over the Arabian Sea.
- The progressive increase in convective activity in the afternoon could be attributed to the cause of the higher τ in the afternoon compared to forenoon dust storm cases. The value of g and α indicated the coarse nature of dust aerosol particles over the Arabian Sea during the dust strom events.

The present study has shown the potential of BT_{31}–BT_{32} in detecting the dust storm, but there may be another combination of bands that might enhance the spatial dust extraction and a detailed study of the different combination of MODIS thermal bands is needed.

Acknowledgements We would like to acknowledge the Indian Institute of Remote Sensing Dehradun for conducting this research work. We express our thanks to Department of Meteorology, Stockholm University for support during the project. We also want to acknowledge NASA for MODIS data.

Compliance with Ethical Standards

Conflict of interest The authors state that there is no conflict of interest. The authors also declare that there is no financial or personal relationship with a third party whose interests could be positively or negatively influenced by this article's content.

References

Ackerman SA (1989) Using the radiative temperature difference at 3.7 and 11 μm to tract dust outbreaks. Remote Sens Environ 27(2):129–133

Ackerman SA (1997) Remote sensing aerosols using satellite infrared observations. J Geophys Res Atmos 102(D14):17069–17079

Al-Maamary HilalMS, Hussein AK, Miqdam TC (2017) Climate change: the game changer in the Gulf Cooperation Council region. Renew Sustain Energy Rev 76:555–576

Babu SS, Moorthy KK, Satheesh SK (2004) Aerosol black carbon over Arabian Sea during intermonsoon and summer monsoon seasons. Geophys Res Lett 31(6):1–5

Baddock MC, Bullard JE, Bryant RG (2009) Dust source identification using MODIS: a comparison of techniques applied to the Lake Eyre Basin, Australia. Remote Sens Environ 113(7):1511–1528

Barcelona Dust Forecast Center (2015) Activity Report 2015. https://dust.aemet.es/about-us/report-2015. Accessed 12 May 2017

Betzer PR, Carder KL, Duce RA, Merrill JT, Tindale NW, Uematsu M, Costello DK, Young RW, Feely RA, Breland JA, Bernstein RE (1988) Long–range transport of giant mineral aerosol particles. Nature 336:568–571

Butt MJ, Assiri ME, Ali MA (2017) Assessment of AOD variability over Saudi Arabia using MODIS Deep Blue products. Environ Pollut 231:143–153

Chen YS, Sheen PC, Chen ER, Liu YK, Wu TN, Yang CY (2004) Effects of Asian dust storm events on daily mortality in Taipei, Taiwan. Environ Res 95(2):151–155. https://doi.org/10.1016/j.envres.2003.08.008

Chou MD, Chan PK, Wang M (2002) Aerosol radiative forcing derived from SeaWiFS-retrieved aerosol optical properties. J Atmos Sci 59(3):748–757

Christopher SA, Jones TA (2010) Satellite and surface-based remote sensing of Saharan dust aerosols. Remote Sens Environ 114(5):1002–1007

Coale KH, Johnson KS, Fitzwater SE, Gordon RM, Tanner S, Chavez FP, Ferioli L, Sakamoto C, Rogers P, Millero F, Steinberg P (1996) A massive phytoplankton bloom induced by an ecosystem-scale iron fertilization experiment in the equatorial Pacific Ocean. Nature 383(6600):495–501

Duan SB, Li ZL, Cheng J, Leng P (2017) Cross-satellite comparison of operational land surface temperature products derived from MODIS and ASTER data over bare soil surfaces. ISPRS J Photogramm Remote Sens 126:1–10

Jafari R, Malekian M (2015) Comparison and evaluation of dust detection algorithms using MODIS Aqua/Terra Level 1B data and MODIS/OMI dust products in the Middle East. Int J Remote Sens 36(2):597–617. https://doi.org/10.1080/01431161.2014.999880

Janugani S, Jayaram V, Cabrera SD, Rosiles JG, Gill TE, Rivera NR (2009) Directional analysis and filtering for dust storm detection in NOAA-AVHRR imagery. In: Algorithms and Technologies for multispectral, hyperspectral, and ultraspectral imagery XV 2009 Apr 27 (vol 7334, p 73341G). International Society for Optics and Photonics

Kaiser J (2005) Mounting evidence indicts fine-particle pollution. Science 307:1858–1861. https://doi.org/10.1126/science.307.5717.1858a

Karimi N, Moridnejad A, Golian S, Vali Samani JM, Karimi D, Javadi S (2012) Comparison of dust source identification techniques over land in the Middle East region using MODIS data. Can J Remote Sens 38(5):586–599. https://doi.org/10.5589/m12-048

Karimi S, Niksokhan MH, Karimi S (2016) Modeling snow cover area and predicting its changes in Haraz catchment. Imaging 2(4):450–455

Kaskaoutis DG, Badarinath KV, Kumar Kharol S, Rani Sharma A, Kambezidis HD (2009) Variations in the aerosol optical properties and types over the tropical urban site of Hyderabad, India. J Geophys Res Atmos 114(D22):1–20

Kiran VR, Talukdar S, Ratnam MV, Jayaraman A (2018) Long-term observations of black carbon aerosol over a rural location in southern peninsular India: role of dynamics and meteorology. Atmos Environ. https://doi.org/10.1016/j.atmosenv.2018.06.020

Kolla V, Biscaye PE (1977) Distribution and origin of quartz in the sediments of the Indian Ocean. J Sediment Res 47(2):642–649

Krishnamurthy V, Kinter JL (2003) The Indian monsoon and its relation to global climate variability. global climate. Springer, Berlin, pp 186–236

Kurosaki Y, Shinoda M, Mikami M (2011) What caused a recent increase in dust outbreaks over East Asia? Geophys Res Lett. https://doi.org/10.1029/2011gl047494

LADSWEB via https://ladsweb.modaps.eosdis.nasa.gov. Accessed 12 June 2016

Lee YC, Yang X, Wenig M (2010) Transport of dusts from East Asian and non-East Asian sources to Hong Kong during dust storm related events 1996–2007. Atmos Environ 44(30):3728–3738. https://doi.org/10.1016/j.atmosenv.2010.03.034

Lee SS, Lee EH, Sohn BJ, Lee HC, Cho JH, Ryoo SB (2017) Improved dust forecast by assimilating MODIS IR-based nighttime AOT in the ADAM2 model. SOLA 13:192–198

Legrand M, Plana-Fattori A, N'doumé C (2001) Satellite detection of dust using the IR imagery of Meteosat: 1. Infrared difference dust index. J Geophys Res Atmos 106(16):18251–18274

Levy RC, Remer LA, Tanré D, Mattoo S, Kaufman YJ (2009) Algorithm for remote sensing of tropospheric aerosol over dark targets from MODIS: collections 005 and 051: Revision 2; Feb 2009. MODIS algorithm theoretical basis document

Li X, Song W (2009) Dust storm detection based on Modis data. In: International conference on geo-spatial solutions for emergency management and the 50th anniversary of the Chinese Academy of surveying and mapping 169–172

MCTK via https://github.com/dawhite/MCTK. Accessed 12 Jan 2017

Martin JH, Coale KH, Johnson KS, Fitzwater SE, Gordon RM, Tanner SJ, Hunter CN, Elrod VA, Nowicki JL, Coley TL, Barber RT (1994) Testing the iron hypothesis in ecosystems of the equatorial Pacific Ocean. Nature 371(6493):123–129

Middleton NJ (1986) A geography of dust storms in South-west Asia. Int J Climatol 6(2):183–196

Moorthy KK, Babu SS, Satheesh SK (2005) Aerosol characteristics and radiative impacts over the Arabian Sea during the intermonsoon season: results from ARMEX field campaign. J Atmos Sci 62(1):192–206

Munir MM, Sasmito B, Haniah H (2015) Analisis Pola Kekeringan Lahan Pertanian Di Kabupaten Kendal Dengan Menggunakan Algoritma Thermal Vegetation Index Dari Citra Satelit Modis Terra. J Geodesi Undip 4(4):174–180

Norton CC, Mosher FR, Hinton B, Martin DW, Santek D, Kuhlow W (1980) A model for calculating desert aerosol turbidity over the oceans from geostationary satellite data. J Appl Meteorol 19(6):633–644

Operational Dust Storm Forecasting at the Met Office. Available via http://forecast.uoa.gr/Dust-wshop-pdf/Brooks.pdf. Accessed 23 Oct 2017

Pease PP, Tchakerian VP, Tindale NW (1998) Aerosols over the Arabian Sea: geochemistry and source areas for aeolian desert dust. J Arid Environ 39(3):477–496

Reed L, Nugent K (2018) The health effects of dust storms in the Southwest United States. Southwest Respir Crit Care Chronicles 6(22):42–46

Sateesh M, Soni VK, Raju PVS (2018) Effect of diwali firecrackers on air quality and aerosol optical properties over mega city (Delhi) in India. Earth Syst Environ. https://doi.org/10.1007/s41748-018-0054-x

Satheesh SK, Moorthy KK (1998) Aerosol characteristics over coastal regions of the Arabian Sea. Oceanogr Lit Rev 3(45):466

Satheesh SK, Moorthy KK, Kaufman YJ, Takemura T (2006) Aerosol optical depth, physical properties and radiative forcing over the Arabian Sea. Meteorol Atmos Phys 91(1–4):45–62

Shao Y (2008) Physics and modelling of wind erosion, vol 37. Springer, Berlin

Shenk WE, Curran RJ (1974) The detection of dust storms over land and water with satellite visible and infrared measurements. Mon Weather Rev 102(12):830–837

Shi GY, Zhao SX (2003) Several scientific issues of studies on the dust storms Chin. J Atmos Sci 27(4):591–606

Singh J (2016) Ranking South African provinces on the basis of MERRA 2D surface incident shortwave flux. J Energy South Afr 27(3):50–57

Sirocko F (1991) Deep-sea sediments of the Arabian Sea: a paleoclimatic record of the southwest-Asian summer monsoon. Geol Rundsch 80(3):557–566

Solmon F, Nair VS, Mallet M (2015) Increasing Arabian dust activity and the Indian summer monsoon. Atmos Chem Phys 15(14):8051–8064

Stocker TF et al (2013) Contribution of Working Group I to the fifth assessment report of the intergovernmental panel on climate change climate change 2013: the physical science basis. Cambridge University Press, Cambridge

Taghavia F, Mohammadi H (2008) The survey of linkage between climate changes and desertification using extreme climate index software. Desert 13(1):9–17

Vincent RF (2018) The effect of Arctic dust on the retrieval of satellite derived sea and ice surface temperatures. Sci Rep 8(1):9727

Wang T, Yan CZ, Song X, Li S (2013) Landsat images reveal trends in the aeolian desertification in a source area for sand and dust storms in China's Alashan plateau (1975–2007). Land Degrad Dev 24(5):422–429

Washington R, Todd M, Middleton NJ, Goudie AS (2003) Dust-storm source areas determined by the total ozone monitoring spectrometer and surface observations. Ann Assoc Am Geogr 93(2):297–313

Xie Y, Zhang W, Qu JJ (2017) Detection of Asian dust storm using MODIS measurements. Remote Sens 9(8):869

Yu M, Yang C (2016) Improving the non-hydrostatic numerical dust model by integrating soil moisture and greenness vegetation fraction data with different spatiotemporal resolutions. PLoS ONE 11(12):e0165616

Yue H, He C, Zhao Y, Ma Q, Zhang Q (2017) The brightness temperature adjusted dust index: an improved approach to detect

dust storms using MODIS imagery. Int J Appl Earth Obs Geoinf 57:166–176

Zhang P, Lu NM, Hu XQ, Dong CH (2006) Identification and physical retrieval of dust storm using three MODIS thermal IR channels. Glob Planet Change 52(1–4):197–206

Zhang B, Tsunekawa A, Tsubo M (2008) Contributions of sandy lands and stony deserts to long-distance dust emission in China and Mongolia during 2000–2006. Glob Planet Change 60(3–4):487–504

Zhu A, Ramanathan V, Li F, Kim D (2007) Dust plumes over the Pacific, Indian, and Atlantic oceans: climatology and radiative impact. J Geophys Res: Atmospheres 112(D16):1–20